http://dx.doi.org/10.5012/bkcs.2012.33.4.1128

Photopatternable Conducting Polymer Nanocomposite with Incorporated Gold Nanoparticles for Use in Organic Field Effect Transistors

Sung Huh, Hyun Ho Choi,† Kilwon Cho,† and Seung Bin Kim*

*Department of Chemistry, Pohang University of Science and Technology, Pohang 790-784, Korea. *E-mail: sbkim@postech.edu*
†Department of Chemical Engineering, Pohang University of Science and Technology, Pohang 790-784, Korea
Received August 10, 2011, Accepted December 19, 2011

We investigated a new method for patterning organic field-effect transistors (OFETs) using a photopatternable conducting polymer nanocomposite, consisting of poly(3-hexylthiophene) (P3HT)-coated gold nanoparticles (AuNPs) that had been modified with a photoreactive cinnamate group, to form P3HT-AuNP-CI. We found that the addition of the cinnamate group to the nanoparticle surface assisted the preparation of a solvent-resistive semiconducting film and preserved the P3HT ordering, which was interrupted by Au-P3HT interactions, as well as provided UV-controllable electrical properties. The P3HT-AuNPs-CI films could be microscale-patterned *via* a UV crosslinking photoreaction, represented as a promising photopatternable semiconductor material for use in advanced applications, with tunable electrical properties for fabrication of sub-micron and microscale electronic devices.

Key Words : Organic field-effect transistors (OFETs), Conducting polymer, Gold nanoparticles, Crystallinity, Electrical characteristics

Introduction

Over the past few decades, the development of organic field effect transistors (OFETs) has received much attention because OFETs are inexpensive to prepare, are easily fabricated over large areas, and are amenable to solution processing.[1-4] In particular, fine strategies for patterning semiconductor devices are required for a wide range of applications. Previous studies have reported various patterning processes for semiconductors, for instance, inkjet printing, nanolithography imprinting, and photolithography.[5-9]

Among these processes, photo-induced pattering methods hold great potential for assembling micro- and nanoscale patterns due to their low cost and simplicity. Generally, photo-induced patterning methods have focused on UV-crosslinkable polymer insulators, such as polyvinyl alcohol, polyvinyl phenol, *etc*.[10,11] It is because of the weakness of the semiconducting films in the general organic solvent, accompanied with damages of the films during the patterning process. Among the methods reported for directly patterning semiconducting films, few include photo-crosslinkable modifications or the addition of a crosslinking agent.[12-14] However, most processes that involve the direct crosslinking of the semiconducting polymer produce disordered regions in the semiconductor crystalline structure, which decrease the device electrical performance. Disruptions in the crystallinity of the active layer should be avoided or minimized to obtain the desired electrical properties during photo-induced patterning.

In this work, we investigated a new photopatternable organic semiconducting layer prepared using a conducting polymer nanocomposite for efficient OFET fabrication. This new nanocomposite includes poly(3-hexylthiophene) (P3HT), which has a high mobility and excellent charge transport properties, gold nanoparticles (AuNPs), and the photoreactive cinnamate group.[15,16] In addition to their rapid and efficient patternability *via* UV irradiation, the films were found to be stable, and the electrical properties could be tuned during the patterning process.

After preparing the P3HT-coated AuNPs (P3HT-AuNPs),[17,18] which were stabilized by strong interactions between sulfur groups of the P3HT and Au, a photoreactive molecule (12,13-dithia-tetracosane-1,24-dicinnamate) (CI) containing a gold nanoparticle capping group and a cinnamate moiety (known for its photochemical reactivity under UV irradiation), was introduced to the P3HT-AuNPs to form P3HT-AuNPs-CI.[19,20] The CI molecules on the surfaces of the AuNPs acted as bridges between the AuNPs to covalently link the nanocomposites within the film, as a result, a photopatternable film was produced *via* selective cross-linking through a shadow mask. Notably, this nanocomposite retained the π-π stacking interactions of the conjugated polymer chain during the crosslinking process, as determined by XRD studies and the UV/vis spectrum, and the electrical properties could be enhanced by adjusting the UV irradiation time. This photopatternable gold nanocomposite is a promising material for the fabrication of conducting polymer/nanoparticle hybrid devices for use in OFETs.

Experimental Section

Materials. Cinnamoyl chloride (98%), bis(11-hydroxyundecyl) disulfide (99%), triethylamine (99%), tetraoctylammonium bromide (99%), gold (II) chloride hydrate (99.999%), and sodium borohydride (98%) were purchased from Aldrich. Poly(3-hexylthiophene-2,5-diyl) was purchas-

ed from Rieke Metals, Inc. All other reagents were used without further purification.

Preparation of P3HT-AuNPs-CI. AuNPs modified with P3HT were prepared using a two-phase system[21,22] with tetraoctylammonium bromide (0.27 g, 0.5 mmol) in toluene (8 mL) as a phase-transfer reagent. Aqueous $HAuCl_4$ (0.039 g, 0.1 mmol) and toluene were mixed, followed by addition of P3HT (0.045 g, 0.1 mmol; Mw = 45,000-50,000) dissolved in 3 mL toluene. With vigorous stirring, an aqueous solution of $NaBH_4$ was added dropwise to the mixture, which was then allowed to react for three hours. The AuNPs were extracted from the organic phase and washed with ethanol. To prepare bifunctional AuNPs, the cinnamate-containing disulfide stabilizer (CI), which was synthesized as reported previously,[18] was introduced to the surface of P3HT-AuNPs *via* an exchange reaction.[23,24] The P3HT-AuNPs (0.022 g, 0.05 mmol P3HT) in toluene (3 mL) were dissolved in 2 mM CI in toluene (5 mL). The solution was stirred for 4 h at 30 °C. The solution contained a 20:1 molar ratio of CI/P3HT.[18] The replacement of P3HT with CI was presumably driven by the high affinity of the sulfur in CI on the AuNPs surface. After the exchange reaction had proceeded to a sufficient degree, the solvent was removed by evaporation, and the product was washed with methanol. The resulting nanocomposite P3HT-AuNPs-CI was characterized by UV/vis spectroscopy and compared with the spectra of P3HT and CI-AuNPs. The immobilization of P3HT and CI on the nanoparticle surfaces was confirmed by Fourier transform infrared (FTIR) and Raman spectroscopies.

Measurements. FTIR spectroscopic measurements were carried out at a spectral resolution of 4 cm^{-1} using a Bomem DA8 FTIR spectrometer equipped with a liquid nitrogen-cooled mercury-cadmium-telluride (MCT) detector. The samples were applied to NaCl windows (25 mm diameter × 2 mm thick) for all FTIR spectra. The UV/vis spectra were obtained using a Shimadzu UV 1601 spectrometer. The UV absorption spectra were measured in dilute chloroform solutions.

The formation of nanoparticles was confirmed by transmission electron microscopy (TEM) measurements. The samples were prepared by evaporating a drop of the P3HT-AuNPs-CI solution (0.1 wt % in toluene) onto an amorphous carbon film supported on a copper grid (400 mesh). The samples were examined using a JEOL2100EX electron microscope operated at 200 KV. Typical phase-contrast images were obtained. The crystallinity of the coated film was analyzed by synchrotron X-ray diffraction at the BL13XU beamline at SPring-8, Japan. The grazing angle, theta, was fixed at 0.18°. The patterned films were characterized by atomic force microscopy (AFM) operated in the non-contact mode (Veeco digital Instruments dimension 3100) and by optical microscopy (OM, Olympus BX51TR).

FET Measurements and Patterning Process. To carry out FET measurements, a 1 wt % ortho-dichlorobenzene solution of the P3HT-AuNPs-CI composites was spin-coated onto the SiO_2/Si wafer for 1 min at 2,000 rpm. The film was dried under vacuum for 24 h, and top-contacted source-drain Au electrodes were deposited by thermal evaporation through a shadow mask onto the active layer. The channel length (L) and width (W) were 100 and 1000 μm. The electrical characteristics of the FETs were measured using a Keithley 2636A sourcemeter. UV irradiation was introduced by illuminating the sample through a shadow mask with a high-pressure 1.0 kW Hg lamp system (Altech, model ALHg-1000) outfitted with a bandpass optical filter (Milles Griot, Model 03-FCG-179) that transmitted 260-380 nm light. The optically filtered UV light intensity was 10 mW/cm^2. The exposure dose was measured using an International Light photometer (model IL 1350) with a sensor (model SED 240). Photo-induced carrier generation was excluded by measuring each device 1 week after UV exposure. The patterned film was obtained by UV exposure through a TEM grid as a shadow mask (square width: 7.5 μm). After removing the TEM grid, the film was washed with toluene briefly and dried. The patterned images were obtained by optical microscopy and AFM.

Results and Discussion

Figure 1(a) shows a simple diagram for the P3HT-AuNPs-CI nanocomposite film on the SiO_2/Si substrate. The nanocomposite consist of AuNPs with two different materials on the particle surface, that is, P3HT and CI molecules. After UV irradiation on the film surface, it can be aggregated each other caused by dimerization of the CI molecules. We found that photo-controllable FET properties of the P3HT-AuNPs-CI devices based on top contact source/drain electrode (Figure 1(b)), as well as the photo-patternability of the film

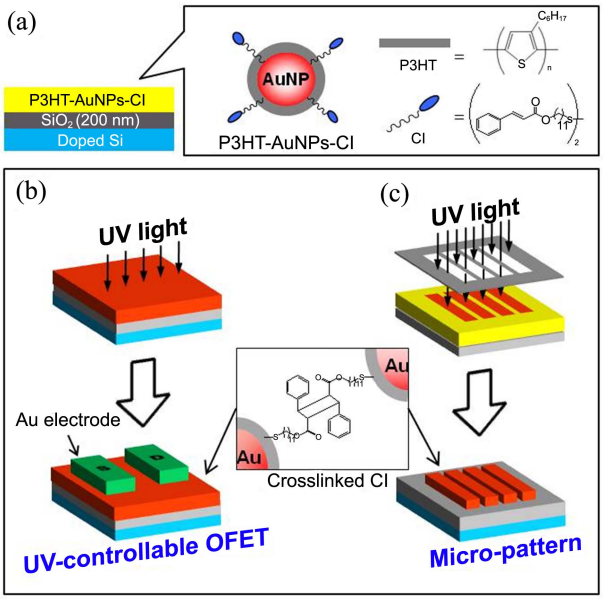

Figure 1. (a) Schematic representation of P3HT-AuNPs-CI nanocomposite film on the SiO_2/Si substrate. (b) Fabrication of P3HT-AuNPs-CI OFET device with the UV-controllability. (c) Photo-induced patterning process of P3HT-AuNPs-CI film and micro-scaled pattern.

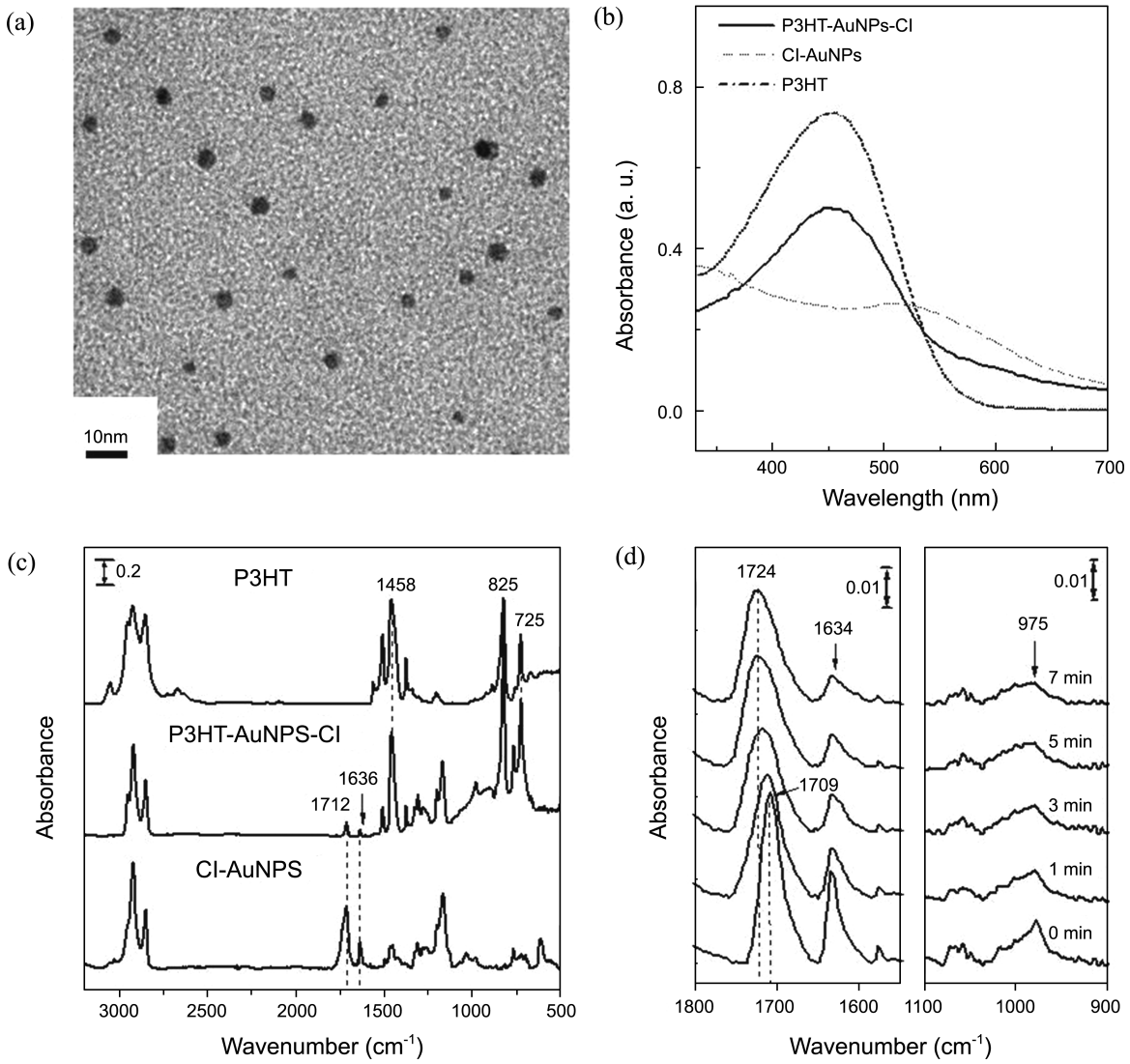

Figure 2. (a) TEM image of a P3HT-AuNPs-CI film. (b) UV/vis spectra of P3HT, CI-AuNPs, and P3HT-AuNPs-CI. (c) FTIR spectra of P3HT, P3HT-AuNPs-CI, and CI-AuNPs. (d) Change of the FTIR spectra of P3HT-AuNPs-CI by UV exposure time.

in the micro-scale, as shown in Figure 1(c).

Figure 2(a) shows a TEM image of P3HT-AuNPs-CI, which shows the well-separated AuNPs of average diameter 3.31 ± 0.43 nm, calculated by collected TEM images including the 95 isolated particles (data not shown). The resulting particles have good solubility in many organic solvents, including chloroform, benzene, and toluene. Figure 2(b) shows the UV/Vis spectra of P3HT, P3HT-AuNPs, and CI-AuNPs. An absorption maximum corresponding to the π-π^* transition of the conjugated polymer chains is observed around 450 nm.[25,26] The absorption from 500 to 600 nm in the P3HT-AuNPs-CI corresponds to both self-orientation of the P3HT on the surface of the nanoparticles[27] and a surface plasmon resonance on the AuNPs,[28] as shown in the spectrum of CI-AuNPs. Therefore, the broad band provides reasonable evidence for the formation of nanoparticles and the immobilization of the polymer on the particle surfaces.

To characterize the chemical structures of P3HT, P3HT-AuNPs-CI, and CI-AuNPs, we obtained the FTIR spectra, as shown in Figure 2(c). P3HT exhibits vibrational bands corresponding to a CH_3 stretching mode at 2955 cm^{-1}, a CH_2 antisymmetric stretching mode at 2927 cm^{-1}, a CH_2 symmetric stretching mode at 2854 cm^{-1}, a C=C ring stretching mode at 1458 cm^{-1}, a CH_2 bending mode at 1377 cm^{-1}, a CH deformation at 824 cm^{-1}, and a =C–S stretching mode at 725 cm^{-1}.[29,30] The bands in the spectrum of P3HT-AuNPs-CI resemble those of P3HT, indicating that P3HT exists on the particles. The peak shift or decrease of vibration of P3HT due to exchanged CI molecules, indicating the replacement of P3HT molecules or interaction between CI and P3OT, was not sufficiently distinctive. It is supposed to be caused by the existence of partially-exchanged P3HT weakly interacting with AuNPs.[31-33] The spectrum of P3HT-AuNPs-CI includes a C=O stretching vibrational mode at 1712 cm^{-1} and a C=C stretching vibrational mode at 1637 cm^{-1}, similar to the spectrum of the CI-AuNPs. Raman spectrum provides spectroscopic evidence for binding of CI molecules on the gold surfaces, indicating the absence of S-S stretching modes

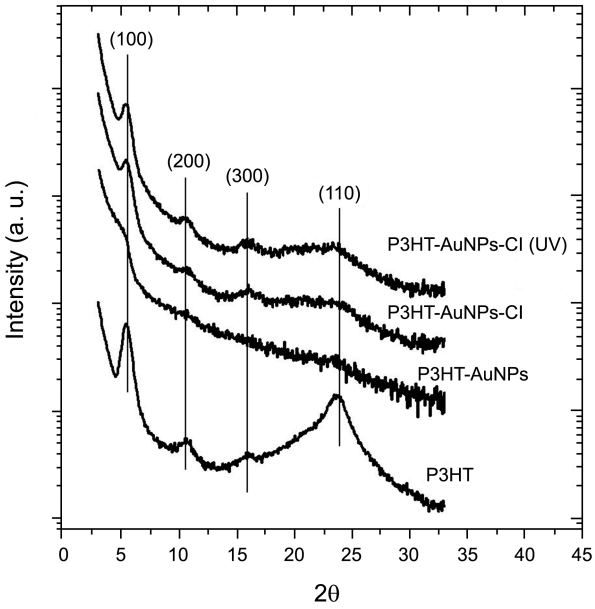

Figure 3. XRD intensities as a function of the scattering angle 2θ for P3HT and P3HT nanocomposite films.

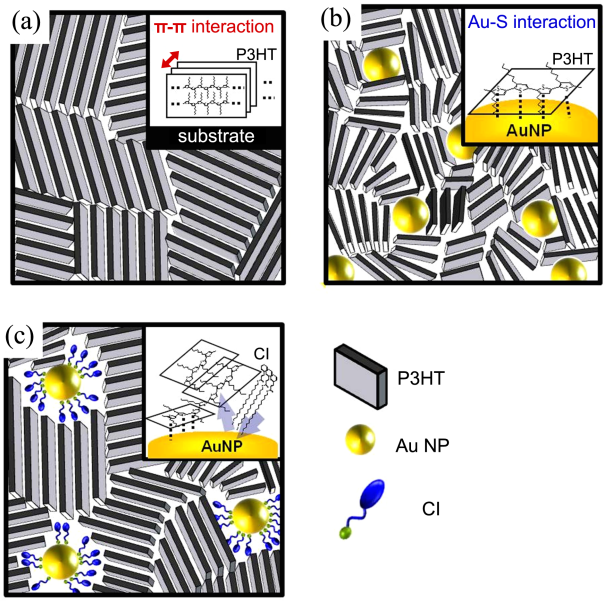

Figure 4. Suggested structure of the interface between AuNPs and P3HT: (a) P3HT, (b) P3HT-AuNPs, and (c) P3HT-AuNPs-CI.

in P3HT-AuNPs-CI.[34] We observed the absence of the band of 504 cm^{-1} related to S-S vibration mode of CI molecule in the Raman spectrum of P3HT-AuNPs-CI (data not shown). Consequently, the results clearly suggest that CI and P3HT were both present on the AuNPs surfaces. Figure 2(d) shows the change in FTIR spectra of P3HT-AuNPs-CI during UV treatment time. The vibrational bands in the spectrum could be assigned in accordance with results reported previously.[35,36] The intensities of the band at 1634 cm^{-1} and 975 cm^{-1} (due to the vinylene C=C stretching vibration and the trans vinylene C–H deformation vibration in the cinnamoyl chromophore, respectively) decrease as the UV exposure time increases. In particular, we can observe the peak shift of the C=O stretching vibration from 1709 to 1724 cm^{-1} with increasing exposure. These observations represent the cleavage of the double bond in the cinnamate group, accompanied by the photocrosslinking reaction.

The molecular structure of P3HT bound to AuNPs was characterized by out-of-plane grazing incidence X-ray diffraction (GIXD) studies of the film, as shown in Figure 3. In the P3HT film, the peak at $2\theta = 5.4°$ and the higher-order peaks correspond to lamellar layered structures that could be assigned to the (100), (200), and (300) planes. The peak at $2\theta = 23.6°$ corresponds to a (010) planar structure, indicating π-π stacking of P3HT. These results show that the P3HT film includes two types of alignments: alignment along the α-axis and along the in-plane direction.[37] The corresponding peaks in the P3HT-AuNP films are reduced in intensity, almost to the point of disappearing. P3HT in these films have low crystallinity due to the disruptive presence of the AuNPs. However, the film crystallinity is recovered in the P3HT-AuNPs-CI and retained after UV treatment.

These interesting observations could be explained by the suggested structural interface between the AuNPs and P3HT, as shown in Figure 4. Homo P3HT presents well-organized lamellar structures due to the π-π stacking among the planar thiophene main chains, uniformly spaced by the alkyl side chains. In contrast, the P3HT chain orientation in P3HT-AuNPs appears to be disrupted by the presence of AuNPs in the film.[38,39] The interactions between Au and sulfur favor the in-plane orientation of backbone chains on the AuNPs surfaces, thereby interrupting the self-orientation of P3HT, leading to disorder among the chains. As the long alkyl chain of the cinnamate groups is introduced to the surface of the AuNPs *via* an exchange reaction, the sulfur groups of the P3HT interact weakly with the AuNP surfaces and are partially removed. As a result, free P3HT is generated and the P3HT chains regain their self-organized structures. It is assumed that the CI molecules help recover the ordering of the P3HT chains, consequently, P3HT-AuNPs-CI shows better crystallinity and orientations than P3HT-AuNPs.

We fabricated FET devices using the nanocomposites and measured their electrical characteristics. Figure 5 shows the transfer characteristics (I_D-V_G) with a fixed drain voltage of –50 V. The average field-effect mobility of each transistor was calculated by plotting the square root of the drain current versus the gate voltage, and the data were fit to the following equation:

$$I_D = \frac{W\mu C_i}{2L}(V_G - V_T)^2, \quad (1)$$

where $C_i = 1.08 \times 10^{-8}$ Fcm^{-2}, $W/L = 20$. The homo P3HT devices performance yielded field-effect mobilites of 2.1×10^{-4} cm^2/Vs and on/off current ratios of ~10^4, similar to previous results.[40] P3HT-AuNPs devices show field-effect mobilities of 1.9×10^{-6} cm^2/Vs and on/off current ratios of ~10^1, about 10^3 times less than the values of the homo P3HT. Notably, P3HT-AuNPs-CI devices show improved electrical performances, with field-effect mobilities of 2.2×10^{-5} cm^2/Vs and on/off current ratios of ~10^3. Apparently, the elec-

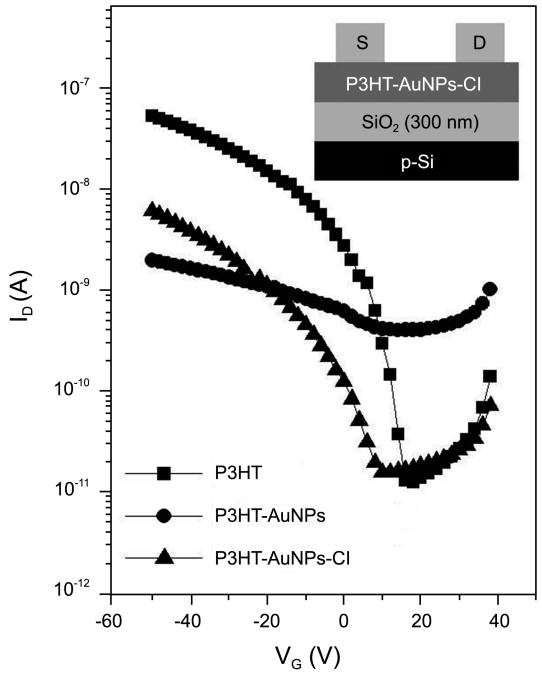

Figure 5. Drain current (I_D) *vs.* gate voltage (V_G) at a fixed V_{DS} of –50 V for P3HT, P3HT-AuNPs, and P3HT-AuNPs-CI FETs. The inset shows a schematic diagram of the devices.

trical characteristics are restored after addition of CI molecules to the AuNP surfaces. As shown in the XRD spectra above (Figure 3), the P3HT chains become disordered due to the spatial disturbance of AuNPs in the P3HT-AuNPs films, leading to a sharp decline of the device performance. The transfer characteristics of P3HT-AuNPs-CI tolerably recover upon introduction of CI to the AuNPs surfaces, which improve the molecular ordering of the P3HT chains.

Another interesting point is the UV-dependent transfer characteristics of the P3HT-AuNPs-CI film for use in OFETs. Figure 6 shows that the electrical performance of the film gradually improved area in the UV exposure time of 0, 1, 3, and 5 min. The mobilities as a function of UV exposure time are displayed in the inset of Figure 6. The trends in mobilities seen here are not observed in the case of the homo P3HT-FET. We could not observe reproducible FET properties after 5-min treatment because of its wide distribution compared to that of before 5-min treatment. It is supposed to be caused by the UV-induced degradation of the CI molecules after the saturation of its photoreaction on the AuNP surface.[36,41] It shows that we can obtain the reasonable electrical mobilities and UV-controllable FET properties of P3HT-AuNPs-CI film from 0 to 5 min-treatment of UV light. The changes in molecular orientation upon UV irradiation were examined by UV/vis spectroscopy of P3HT and P3HT-AuNPs-CI films, as shown in Figure 7. An identical absorption peak corresponding to the π-π* transition of the conjugated P3HT chains are observed at 560 nm, and the shoulders at 520 and 605 nm indicate that the π-π stacking of the main chains is preserved, suggesting uniform orientation in the film.[42,43] A slight decrease in the bands related to chain orientation are observed in the absorption spectra as the UV exposure time increased. The inset shows the absorbance decrease at 559 nm and 560 nm in each spectrum upon UV

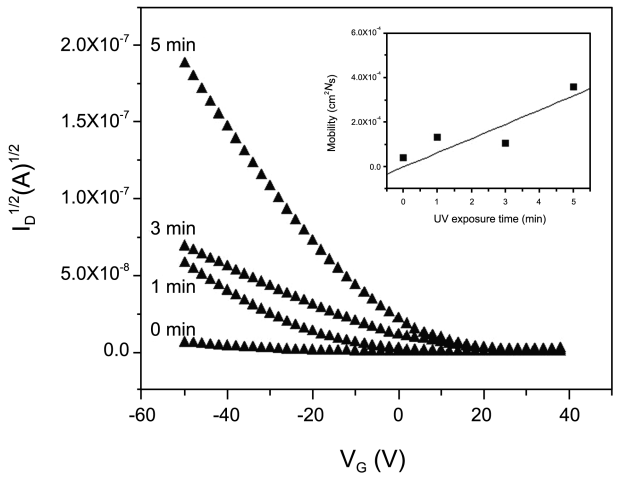

Figure 6. Output characteristics of a P3HT-AuNPs-CI film for use in an OFET as a function of UV irradiation time. The mobilities as a function of UV exposure time are displayed in the inset.

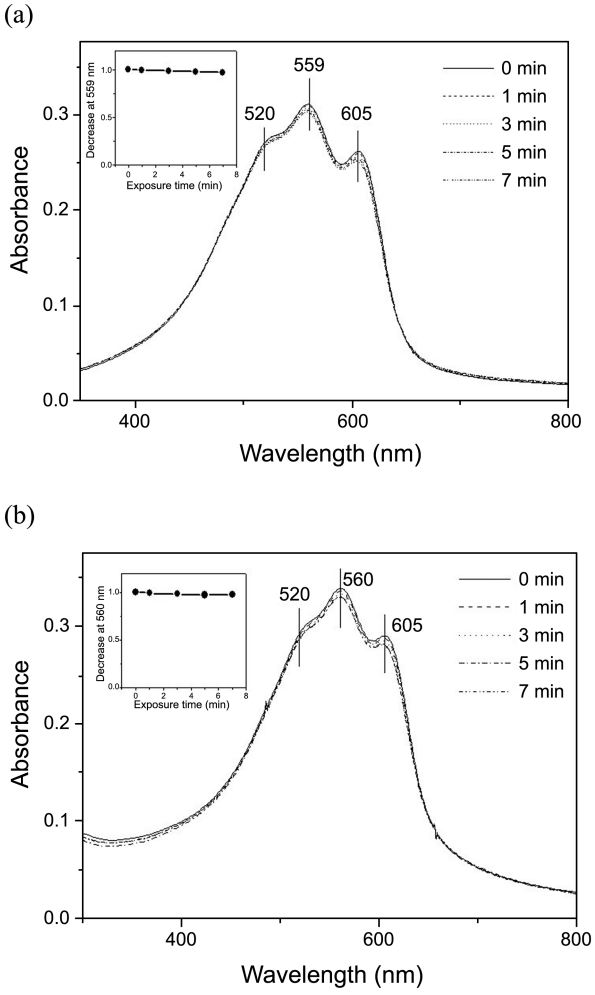

Figure 7. UV/vis spectra of (a) P3HT and (b) P3HT-AuNPs-CI films as a function of UV irradiation. The inset shows an absorbance decrease at 559 nm and 560 nm upon UV irradiation.

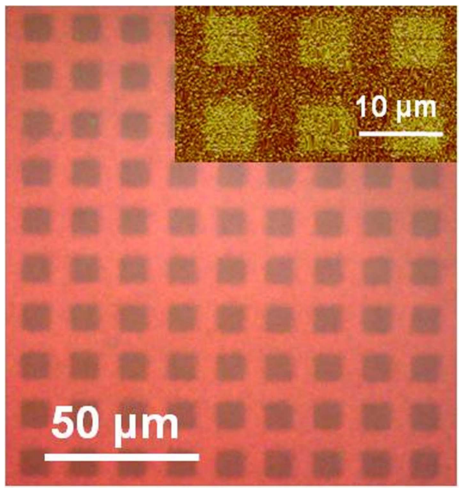

Figure 8. Patterned images of P3HT-AuNPs-CI film by OM and AFM.

irradiation. The results reveal that the conjugation length and crystal ordering were apparently retained, even upon UV irradiation. These conclusions are supported by the XRD spectra in Figure 3, which indicate the retention of crystallinity in the P3HT-AuNPs-CI after UV treatment. In fact, it shows unexpected results that the semiconductor layer holds not only structural stability during crosslinking of the cinnamate groups on the AuNPs surface but also enhanced device performance upon UV exposure variation. The general crosslinked chemical structure, representing the covalently bonded cinnamate groups on AuNPs surfaces is shown in the photo-induced patterning process of P3HT-AuNPs-CI (Figure (8)).[19] It is assumed that the crosslinking procedure causes the slight movement and rearrangement of AuNPs in the solid film, leading to the increase in the self-orientation of the P3HT. A more detailed study is desired to understand the UV treatment effect on the device performance of the new semiconductor film in the next project.

As shown in Figure 1, P3HT-AuNPs-CI thin film on a substrate could be patterned directly by applying UV irradiation through a shadow mask. The exposed area of the film remained and the masked area was removed during the lift-off process with toluene. Selective crosslinking of the nanoparticles through the mask provides a patterned surface. UV exposure for varying lengths of time shows that the patterned features are clearest for an irradiation time of 5 min. Figure 8 shows an optical microscopy image of the patterned P3HT-AuNPs-CI thin film with thickness of several tens of nanometers obtained after UV irradiation. The inset shows an AFM image of the pattern. We plan to continue this work by fabricating improved photopatternable FET devices using the patterned nanocomposite thin films as OFET channels. For this purpose, the patterning processes will be optimized to control the electrical characteristics.

Conclusions

In summary, a new photopatternable conducting polymer nanocomposite P3HT-AuNPs-CI containing photoreactive AuNPs was developed for the fabrication of OFET devices. P3HT-AuNPs-CI films were micro-scale patterned on the SiO_2/Si substrate by UV irradiation, and they maintain a stable molecular structure during the photoreaction. Moreover, π-π stacking among the conjugated polymer chains recovered after introduction of the CI molecules to the AuNPs surfaces. In particular, we found that the electrical properties of the nanocomposite could be improved by controlling the UV irradiation time. Therefore, our results represent the development of potential electronic device applications of conducting polymer-based nanomaterials, achieving the effective modulation of electrical performances.

Acknowledgments. This study was supported by the Second Stage Brain Korea 21 Project.

References

1. Sekitani, T.; Takamiya, M.; Noguchi, Y.; Nakano, S.; Kato, Y.; Sakurai, T.; Someya, T. *Nat Mater.* **2007**, *6*, 413-417.
2. Newman, C. R.; Frisbie, C. D.; da Silva, D. A.; Bredas, J. L.; Ewbank, C. P.; Mann, K. R. *Chem. Mater.* **2004**, *16*, 4436-4451.
3. Chabinyc, M. L.; Wong, W. S.; Salleo, A.; Paul, K. E.; Street, R. A. *Appl. Phys. Lett.* **2002**, *81*, 4260-4262.
4. Liu, S.; Briseno, A. L.; Mannsfeld, S. C. B.; You, W.; Locklin, J.; Lee, H. W.; Xia, Y.; Bao, Z. *Adv. Funct. Mater.* **2007**, *17*, 2891-2896.
5. Wu, C. C.; Marcy, D.; Lu, M. H.; Sturm, J. C. *Appl. Phys. Lett.* **1998**, *72*, 519-521.
6. Behl, M.; Seekamp, J.; Wankovych, S.; Torres, C. M. S.; Zentel, R.; Ahopelto, J. *Adv. Mater.* **2002**, *14*, 588-591.
7. Hua, F.; Sun, Y.; Gaur, A.; Meitl, M. A.; Bilhaut, L.; Rotkina, L.; Wang, J.; Geil, P.; Shim, M.; Rogers, J. A.; Shim, A. *Nano Lett.* **2004**, *4*, 2467-2471.
8. Muller, C. D.; Falcou, A.; Reckefuss, N.; Rojahn, M.; Wiederhirn, V.; Rudati, P.; Frohne, H.; Nuyken, O.; Becker, H.; Meerholz, K. *Nature* **2003**, *421*, 829-833.
9. Gates, B. D.; Xu, Q.; Stewart, M.; Ryan, D.; Willson, C. G.; Whitesides, G. M. *Chem. Rev.* **2005**, *105*, 1171-1196.
10. Yoon, M.-H.; Yan, H.; Facchetti, A.; Marks, T. J. *J. Am. Chem. Soc.* **2005**, *127*, 10388-10390.
11. Peng, X.; Horowitz, G.; Fichou, D.; Ganier, F. *Appl. Phys. Lett.* **1990**, *57*, 2013-2015.
12. Touwslager, F. J.; Willard, N. P.; de Leeuw, E. M. *Appl. Phys. Lett.* **2002**, *81*, 4556-4558.
13. Weidkamp, K. P; Afzali, A.; Tromp, R. M.; Hamers, R. J. *J. Am. Chem. Soc.* **2004**, *126*, 12740-12741.
14. Charas, A.; Alccer, L.; Pimentel, A.; Conde, J. P.; Morgado, J. *Chem. Phys. Lett.* **2008**, *455*, 189-191.
15. Sirringhaus, H.; Brown, P. J.; Friend, R. H.; Nielsen, M. M.; Bechgaard, K.; Langeveld-Voss, B. M. W.; Spiering, A. J. H.; Janssen, R. A. J.; Meijer, E. W.; Herwig, P.; deLeeuw, D. M. *Nature* **1999**, *401*, 685-688.
16. Ma, W.; Yang, C.; Gong, X.; Lee, K.; Heeger, A. J. *Adv. Funct. Mater.* **2005**, *15*, 1617-1622.
17. Zhai, L.; McCullough, R. D., *J. Mater. Chem.* **2004**, *14*, 141-143.
18. Huh, S.; Kim, S. B. *J. Phys. Chem. C* **2010**, *114*, 2880-2885.
19. Egerton, P. L.; Hyde, E. M.; Trigg, J.; Payne, A.; Mijovic, M. V.; Reiser, A., *J. Am. Chem. Soc.* **1981**, *103*, 3859-3863.
20. Huh, S.; Chae, B.; Kim, S. B. *J. Colloid Interface Sci.* **2008**, *327*, 211-215.
21. Brust, M.; Walker, M.; Bethell, D.; Schiffrin, D. J.; Whyman, R. J. *Chem. Soc. Chem. Commun.* **1994**, *7*, 801-802.

22. Brust, M.; Fink, J.; Bethell, D.; Schiffrin, D. J.; Kiely, C. *J. Chem. Soc. Chem. Commun.* **1995**, *16*, 1655-1656.
23. Glogowaski, E.; He, J.; Russell, T. P.; Emrick, T. *Chem. Commun.* **2005**, 4050-4052.
24. Elsenbaumer, R. L.; Shackeltte, L. W. In *Handbook of Conducting Polymers*; Skotheim, T. A., Ed.; Marcel Dekker, Inc.: New York, Vol 1, 1986.
25. Jenekhe, S. A. *Nature* **1986**, *322*, 345-347.
26. Chung, T.-C.; Kaufman, J. H.; Heeger, A. J.; Wudl, F. *Phys. Rev. B* **1984**, *30*, 702-710.
27. McCullough, R. D.; Tristram-Nagle, S. P.; Lowe, R. D.; Jayaraman, M. *J. Am. Chem. Soc.* **1993**, *115*, 4910-4911.
28. Daniel, M. C.; Astruc, D. *Chem. Rev.* **2004**, *104*, 293-346.
29. Yong, C.; Renyuan, Q. *Sol. St. Commun.* **1985**, *54*, 211-213.
30. Teng, M. Y.; Lee, K. R.; Liaw, D. J.; Lai, J. Y. *Polymer* **2000**, *41*, 2047-2052.
31. In general, several interactions contribute to the place exchange reaction on the gold nanoparticle surface such as gold-thiol, incoming thiol-bound thiolate, and incoming thiol-surface monolayer interactions.
32. Hostetler, M. J.; Templeton, A. C.; Murray, R. W. *Langmuir* **1999**, *15*, 3782-3789.
33. Templeton, A. C.; Hostetler, M. J.; Kraft, C. T.; Murray, R. W. *J. Am. Chem. Soc.* **1998**, *120*, 1906-1911.
34. Porter, L. A., Jr.; Ji, D.; Westcott, S. L.; Graupe, M.; Czernuszewicz, R. S.; Halas, N. J.; Lee, T. R. *Langmuir* **1998**, *14*, 7378-7386.
35. Perny, S.; Barny, P. L. *Liq. Cryst.* **2000**, *27*, 329-340.
36. Chae, B.; Lee, S. W.; Jung, Y. M.; Ree, M.; Kim, S. B. *Langmuir* **2003**, *19*, 687-695.
37. Prosa, T. J.; Winokur, M. J.; Moulton, J.; Smith, P.; Heeger, A. J. *Macromolecules* **1992**, *25*, 4364-4372.
38. Ruiz, V.; Nicholson, P. G.; Jollands, S.; Thomas, P. A.; Macpherson, J. V.; Unwin, P. R. *J. Phys. Chem. B* **2005**, *109*, 19335-19344.
39. Nicholson, P. G.; Ruiz, V.; Macpherson, J. V.; Unwin, P. R. *Phys. Chem. Chem. Phys*. **2006**, *8*, 5096-5105.
40. Park, Y. D.; Lim, J. A.; Kwak, D.; Cho, J. H.; Cho, K. *Electrochem. Solid-State Lett.* **2009**, *12*, H312-H314.
41. Trajkovska, A.; Kim, C.; Marshall, K. L.; Mourey, T. H.; Chen, S. H. *Macromolecules* **2006**, *39*, 6983-6989.
42. Sandberg, H.; Frey, G.; Shkunov, M.; Sirringhaus, H.; Friend, R. H. *Langmuir* **2002**, *18*, 10176-10182.
43. Zen, A.; Saphiannikova, M.; Neher, D.; Asawapirom, U.; Scherf, U. *Chem. Mater.* **2005**, *17*, 781-786.